

Supplement of The Cryosphere, 12, 3045–3065, 2018
<https://doi.org/10.5194/tc-12-3045-2018-supplement>
© Author(s) 2018. This work is distributed under
the Creative Commons Attribution 4.0 License.



Supplement of

Dual-satellite (Sentinel-2 and Landsat 8) remote sensing of supraglacial lakes in Greenland

Andrew G. Williamson et al.

Correspondence to: Andrew G. Williamson (agw41@alumni.cam.ac.uk)

The copyright of individual parts of the supplement might differ from the CC BY 4.0 License.

S1 Calculating the values of g

We followed the methods of Pope *et al.* (2016; their Supplement) to calculate the coefficient for the losses in upward and downward travel through the water column (g ; m^{-1}) for the red and green bands of Sentinel-2. The relationship from Smith and Baker (1981; their Eq. (5)) states that:

$$K_d = a + \frac{1}{2}b, \quad (\text{S1})$$

where K_d is the diffuse attenuation coefficient for the clearest natural freshwaters, a is the absorption coefficient for pure water, and b is the backscattering coefficient for molecular (Rayleigh) scattering in freshwater.

We then used the relationship from Sneed and Hamilton (2007; their Eq. (3)), which indicates that:

$$g \approx K_d + aD_u, \quad (\text{S2})$$

where D_u is an upwelling light distribution or the reciprocal of the upwelling average cosine (Mobley, 1994). Since $K_d \approx aD_u$ (Maritorena *et al.*, 1994), g can simply be calculated (using measured values of a and b) with the following:

$$g = 2(K_d), \quad (\text{S3})$$

meaning that Eq. (S1) could then be used to derive the following relationship:

$$g = 2\left(a + \frac{1}{2}b\right). \quad (\text{S4})$$

For a , we followed Pope *et al.* (2016) and took the value from Pope and Fry (1997; their Table 3) to replace that from Smith and Baker (1981; their Table 1), and, for b , we took the value from Buiteveld *et al.* (1994; their Table 1) for each wavelength of Sentinel-2's red and green bands. This allowed a preliminary g value to be calculated for each of Sentinel-2's red and green bands by using Eq. (S4) for each wavelength of the red band (from 646–684 nm in 1 nm increments) and green band (from 537–582 nm in 1 nm increments). To derive final g values for each band, following Pope *et al.* (2016), Sentinel-2's spectral response function (ESA, 2017) was used, akin to the data available for Landsat 8 (Barsi *et al.*, 2014), and average weighted values were calculated according to the spectral response for each wavelength of the red and green bands.

This produced final g values for Sentinel-2's red band of 0.8304 and for Sentinel-2's green band of 0.1413, which compared with the lower g values for Landsat 8's red band of 0.7507 and for Landsat 8's green band of 0.1279 (Pope *et al.*, 2016).

Table S1: Details of Sentinel-2 Multispectral Instrument images used in the study. Cloud cover was determined from the image metadata, representing the percentage of cloud-covered pixels both within the ice-sheet area and off the ice-sheet edge. Data cover was determined from the image metadata, representing the percentage of the total area of the region (i.e. the area on the ice sheet plus the ice-marginal area) for which satellite data were collected.

| Scene ID | UTM zone | Latitude band | Square | Date | Year | Sequence | Cloud cover (%) | Data cover (%) |
|--|----------|---------------|--------|--------|------|----------|-----------------|----------------|
| S2A_OPER_MSI_L1C_DS_MTI__20160502T202602_S20160502T151916_N02.01 | 22N | W | EC | 02 May | 2016 | 0 | 38.9 | 100.0 |
| S2A_OPER_MSI_L1C_DS_SGS__20160505T205541_S20160505T152915_N02.02 | 22N | W | EC | 05 May | 2016 | 0 | 44.7 | 100.0 |
| S2A_OPER_MSI_L1C_DS_MTI__20160515T203516_S20160515T152912_N02.02 | 22N | W | EC | 15 May | 2016 | 0 | 5.4 | 100.0 |
| S2A_OPER_MSI_L1C_DS_SGS__20160518T210306_S20160518T154153_N02.02 | 22N | W | EC | 18 May | 2016 | 0 | 31.4 | 38.3 |
| S2A_OPER_MSI_L1C_DS_MTI__20160522T202416_S20160522T151915_N02.02 | 22N | W | EC | 22 May | 2016 | 0 | 29.8 | 100.0 |
| S2A_OPER_MSI_L1C_DS_MTI__20160529T201543_S20160529T150918_N02.02 | 22N | W | EC | 29 May | 2016 | 0 | 66.1 | 94.3 |
| S2A_OPER_MSI_L1C_DS_SGS__20160601T173946_S20160601T151916_N02.02 | 22N | W | EC | 01 Jun | 2016 | 0 | 18.1 | 99.9 |
| S2A_OPER_MSI_L1C_DS_MTI__20160604T203539_S20160604T152915_N02.02 | 22N | W | EC | 04 Jun | 2016 | 0 | 60.0 | 99.9 |
| S2A_OPER_MSI_L1C_DS_SGS__20160608T202646_S20160608T150916_N02.02 | 22N | W | EC | 08 Jun | 2016 | 0 | 16.2 | 94.2 |
| S2A_OPER_MSI_L1C_DS_MTI__20160611T202435_S20160611T151937_N02.02 | 22N | W | EC | 11 Jun | 2016 | 0 | 42.5 | 100.0 |
| S2A_OPER_MSI_L1C_DS_SGS__20160617T192017_S20160617T153910_N02.04 | 22N | W | EC | 17 Jun | 2016 | 0 | 25.7 | 38.9 |
| S2A_OPER_MSI_L1C_DS_SGS__20160618T202441_S20160618T151305_N02.04 | 22N | W | EC | 18 Jun | 2016 | 0 | 46.7 | 93.2 |
| S2A_OPER_MSI_L1C_DS_MTI__20160621T220258_S20160621T151912_N02.04 | 22N | W | EC | 21 Jun | 2016 | 0 | 4.3 | 100.0 |
| S2A_OPER_MSI_L1C_DS_MTI__20160624T203434_S20160624T152911_N02.04 | 22N | W | EC | 24 Jun | 2016 | 0 | 16.0 | 100.0 |
| S2A_OPER_MSI_L1C_DS_SGS__20160628T202858_S20160628T150914_N02.04 | 22N | W | EC | 28 Jun | 2016 | 0 | 0.1 | 94.0 |
| S2A_OPER_MSI_L1C_DS_MTI__20160701T202434_S20160701T151913_N02.04 | 22N | W | EC | 01 Jul | 2016 | 0 | 73.3 | 100.0 |
| S2A_OPER_MSI_L1C_DS_SGS__20160707T192822_S20160707T153908_N02.04 | 22N | W | EC | 07 Jul | 2016 | 0 | 0.0 | 38.6 |
| S2A_OPER_MSI_L1C_DS_SGS__20160708T202909_S20160708T151305_N02.04 | 22N | W | EC | 08 Jul | 2016 | 1 | 1.6 | 94.2 |
| S2A_OPER_MSI_L1C_DS_SGS__20160711T203749_S20160711T151912_N02.04 | 22N | W | EC | 11 Jul | 2016 | 0 | 0.1 | 100.0 |
| S2A_OPER_MSI_L1C_DS_MTI__20160714T203553_S20160714T152910_N02.04 | 22N | W | EC | 14 Jul | 2016 | 0 | 0.3 | 99.9 |
| S2A_OPER_MSI_L1C_DS_SGS__20160718T202939_S20160718T150915_N02.04 | 22N | W | EC | 18 Jul | 2016 | 0 | 23.7 | 94.2 |

| Scene ID | UTM zone | Latitude band | Square | Date | Year | Sequence | Cloud cover (%) | Data cover (%) |
|--|----------|---------------|--------|--------|------|----------|-----------------|----------------|
| S2A_OPER_MSI_L1C_DS_MTI__20160721T202530_S20160721T151913_N02.04 | 22N | W | EC | 21 Jul | 2016 | 0 | 0.0 | 100.0 |
| S2A_OPER_MSI_L1C_DS_SGS__20160724T205100_S20160724T153051_N02.04 | 22N | W | EC | 24 Jul | 2016 | 0 | 0.0 | 99.9 |
| S2A_OPER_MSI_L1C_DS_SGS__20160727T192945_S20160727T153910_N02.04 | 22N | W | EC | 27 Jul | 2016 | 0 | 0.0 | 38.2 |
| S2A_OPER_MSI_L1C_DS_SGS__20160728T202436_S20160728T151306_N02.04 | 22N | W | EC | 28 Jul | 2016 | 0 | 63.6 | 94.3 |
| S2A_OPER_MSI_L1C_DS_SGS__20160731T203724_S20160731T151913_N02.04 | 22N | W | EC | 31 Jul | 2016 | 0 | 0.0 | 100.0 |
| S2A_OPER_MSI_L1C_DS_MTI__20160803T203554_S20160803T152910_N02.04 | 22N | W | EC | 03 Aug | 2016 | 0 | 3.1 | 100.0 |
| S2A_OPER_MSI_L1C_DS_MTI__20160806T204409_S20160806T153909_N02.04 | 22N | W | EC | 06 Aug | 2016 | 0 | 14.1 | 38.1 |
| S2A_OPER_MSI_L1C_DS_SGS__20160807T202758_S20160807T150914_N02.04 | 22N | W | EC | 07 Aug | 2016 | 0 | 55.9 | 94.4 |
| S2A_OPER_MSI_L1C_DS_MTI__20160810T202535_S20160810T151912_N02.04 | 22N | W | EC | 10 Aug | 2016 | 0 | 13.0 | 100.0 |
| S2A_OPER_MSI_L1C_DS_SGS__20160813T204833_S20160813T153046_N02.04 | 22N | W | EC | 13 Aug | 2016 | 0 | 0.0 | 100.0 |
| S2A_OPER_MSI_L1C_DS_SGS__20160817T202447_S20160817T151257_N02.04 | 22N | W | EC | 17 Aug | 2016 | 0 | 0.7 | 94.4 |
| S2A_OPER_MSI_L1C_DS_MTI__20160830T202522_S20160830T151909_N02.04 | 22N | W | EC | 30 Aug | 2016 | 0 | 2.2 | 100.0 |
| S2A_OPER_MSI_L1C_DS_SGS__20160902T204312_S20160902T153051_N02.04 | 22N | W | EC | 02 Sep | 2016 | 0 | 0.7 | 100.0 |
| S2A_OPER_MSI_L1C_DS_SGS__20160906T202733_S20160906T151257_N02.04 | 22N | W | EC | 06 Sep | 2016 | 0 | 35.9 | 94.5 |
| S2A_OPER_MSI_L1C_DS_SGS__20160909T203815_S20160909T151907_N02.04 | 22N | W | EC | 09 Sep | 2016 | 0 | 21.0 | 100.0 |
| S2A_OPER_MSI_L1C_DS_MTI__20160912T203709_S20160912T152817_N02.04 | 22N | W | EC | 12 Sep | 2016 | 0 | 0.0 | 100.0 |
| S2A_OPER_MSI_L1C_DS_SGS__20160915T210159_S20160915T154130_N02.04 | 22N | W | EC | 15 Sep | 2016 | 0 | 1.7 | 38.2 |
| S2A_OPER_MSI_L1C_DS_MTI__20160926T201345_S20160926T150955_N02.04 | 22N | W | EC | 26 Sep | 2016 | 0 | 0.3 | 93.9 |

Table S2: Details of Landsat 8 Operational Land Imager images used in the study. Cloud cover was calculated as the percentage of pixels both on and off the ice sheet that were obscured by clouds (i.e. those with a band-6 or SWIR value > 0.100; Sect. 2.2.1). Data cover was calculated as a percentage of the total area of the region (i.e. the area on the ice sheet plus the ice-marginal area) for which satellite data had been collected. The asterisk denotes that the image was used for comparing lake areas calculated from the two satellites and for validating the lake depths from Sentinel-2, but that the image was not used for lake tracking because a contemporaneous higher-resolution, and therefore more favourable, Sentinel-2 image was available.

| Scene ID | Path | Row | Date | Year | Cloud cover (%) | Data cover (%) |
|-----------------------|------|-----|---------|------|-----------------|----------------|
| LC80100112016149LGN01 | 010 | 011 | 28 May | 2016 | 85.9 | 95.1 |
| LC80080112016151LGN01 | 008 | 011 | 30 May | 2016 | 8.4 | 72.8 |
| LC80822332016157LGN01 | 082 | 233 | 05 Jun | 2016 | 17.3 | 100.0 |
| LC80090112016158LGN01 | 009 | 011 | 06 Jun | 2016 | 21.6 | 100.0 |
| LC80100112016165LGN01 | 010 | 011 | 13 Jun | 2016 | 43.9 | 95.3 |
| LC80090112016174LGN01 | 009 | 011 | 22 Jun | 2016 | 33.9 | 100.0 |
| LC80100112016181LGN01 | 010 | 011 | 29 Jun | 2016 | 35.0 | 95.2 |
| LC80080112016183LGN01 | 008 | 011 | 01 Jul* | 2016 | 60.8 | 72.6 |
| LC80100112016197LGN01 | 010 | 011 | 15 Jul | 2016 | 21.0 | 95.1 |
| LC80812332016198LGN01 | 081 | 233 | 16 Jul | 2016 | 19.0 | 93.7 |
| LC80080112016199LGN01 | 008 | 011 | 17 Jul | 2016 | 5.9 | 72.8 |
| LC80100112016213LGN01 | 010 | 011 | 31 Jul* | 2016 | 18.5 | 95.2 |
| LC80080112016215LGN01 | 008 | 011 | 02 Aug | 2016 | 12.2 | 72.6 |
| LC80090112016222LGN01 | 009 | 011 | 09 Aug | 2016 | 18.4 | 100.0 |
| LC80100112016229LGN01 | 010 | 011 | 16 Aug | 2016 | 18.3 | 95.2 |
| LC80080112016231LGN01 | 008 | 011 | 18 Aug | 2016 | 6.5 | 72.7 |
| LC80080112016247LGN01 | 008 | 011 | 03 Sep | 2016 | 8.8 | 73.2 |

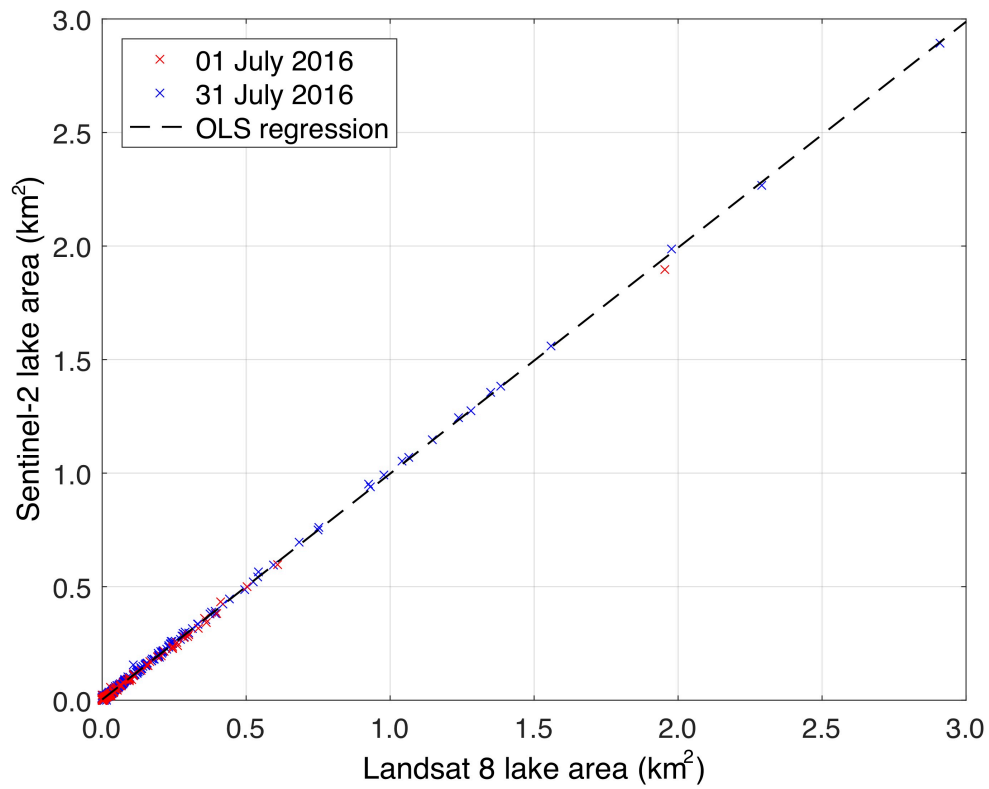


Figure S1: The very strong relationship between Landsat 8 and Sentinel-2 lake areas for the days of overlapping imagery (1 July and 31 July) in 2016. The 594 lake areas used for comparisons were derived using the Normalised Difference Water Index approach with threshold values of 0.25 for both types of imagery. The black dashed line shows an ordinary least-squares (OLS) linear regression, which can explain 99.9% ($R^2 = 0.999$; $p = 0.000$) of the variance in the data. The root-mean square error of 0.007 km² (i.e. seven Sentinel-2 pixels) between the two sets of lake areas is therefore remarkably small.

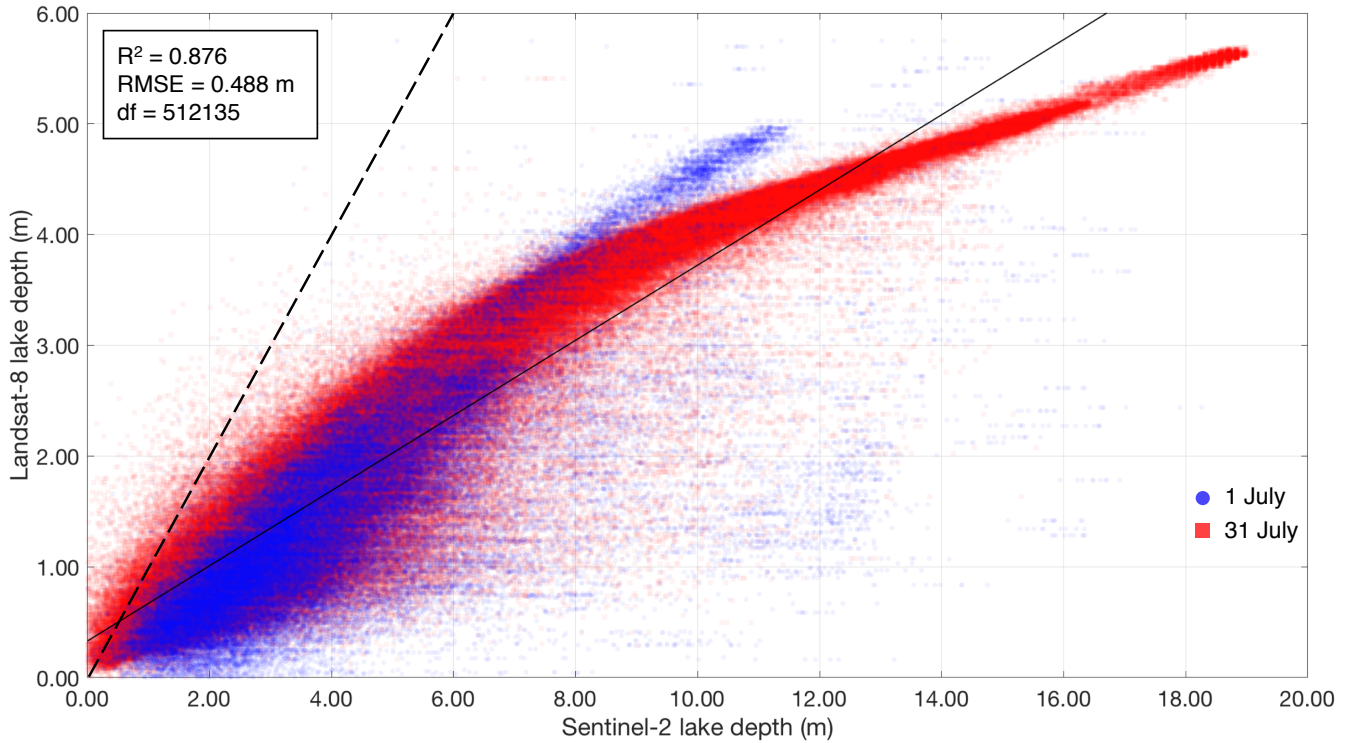


Figure S2: Comparison of lake depths calculated using the physically based method for Sentinel-2 (with the green band) and for Landsat 8 (with the average depths from the red and panchromatic bands). Degrees of freedom (“df” in this figure) = 512,135. The solid black line shows an OLS linear regression and the dashed black line shows a 1:1 relation. The R^2 value indicates that the regression explains 87.6% of the variance in the data. The RMSE of 0.488 m shows the error associated with calculating the Sentinel-2 lake depths using this relationship.

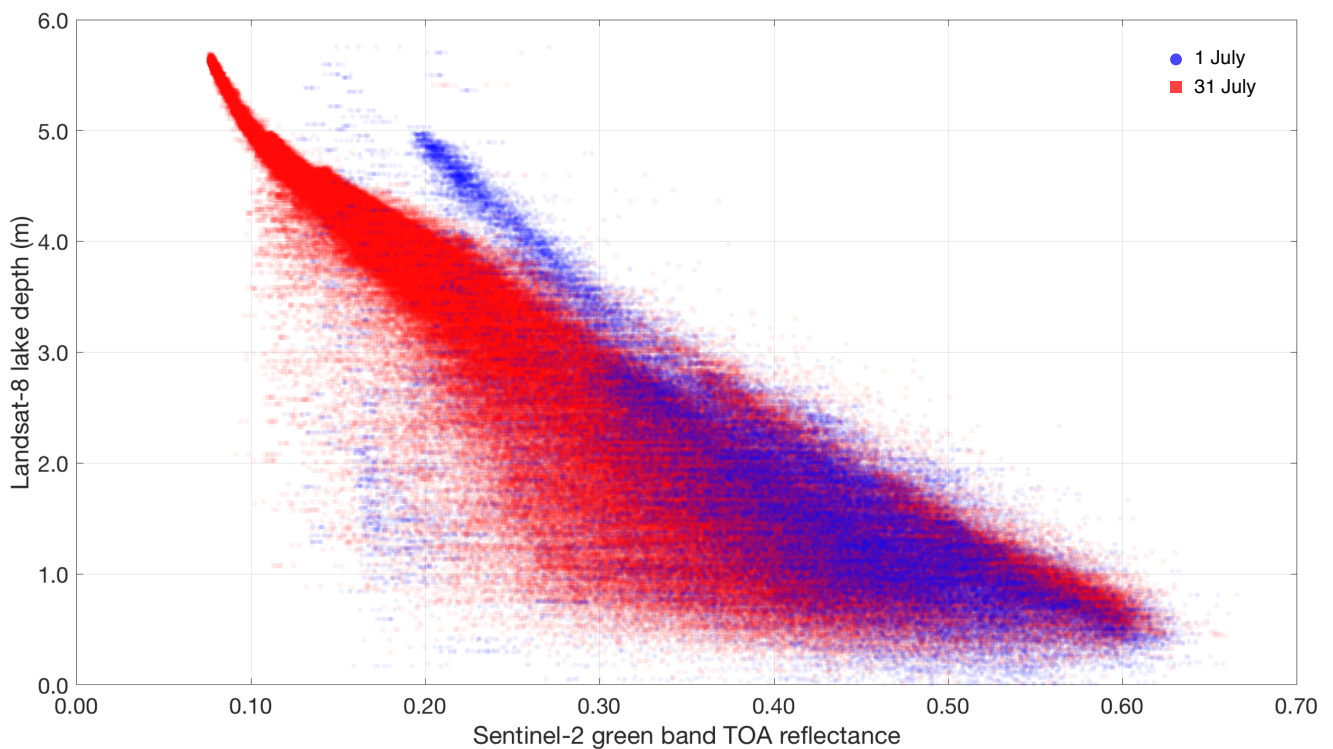


Figure S3: Scatter plot to show the relationship between Sentinel-2 green band top-of-atmosphere (TOA) reflectance and Landsat 8 lake depth for 430,650 data points.

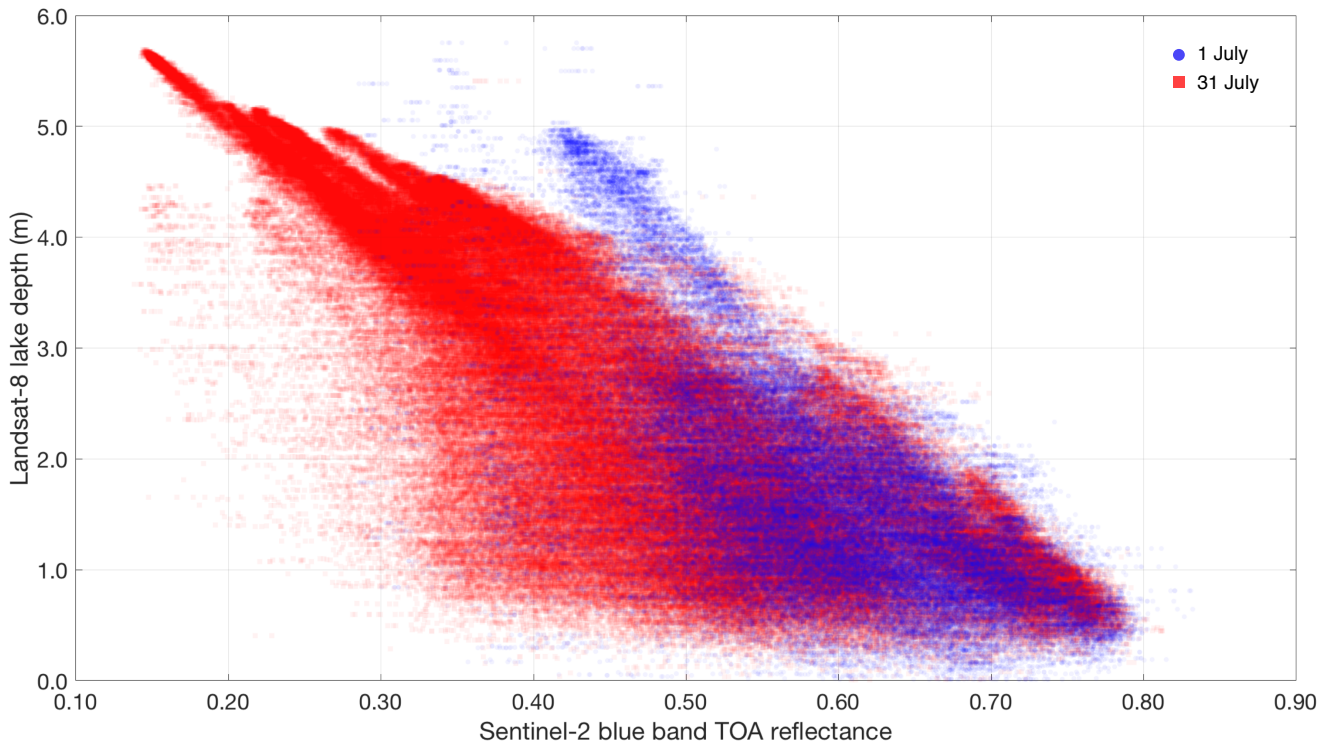


Figure S4: Scatter plot to show the relationship between Sentinel-2 blue band TOA reflectance and Landsat 8 lake depth for 430,650 data points.

References

- Barsi, J. A., Lee, K., Kvaran, G., Markham, B. L., and Pedelty, J. A.: The spectral response of the Landsat-8 Operational Land Imager, *Remote Sens.*, 6, 10232–10251, <https://doi.org/10.3390/rs61010232>, 2014.
- ESA: Sentinel-2 spectral response functions (S2-SRF), accessed 19 February 2018, https://earth.esa.int/web/sentinel/user-guides/sentinel-2-msi/document-library/-/asset_publisher/Wk0TKajiISaR/content/sentinel-2a-spectral-responses, 2017.
- Maritorena, S., Morel, A., and Gentili, B.: Diffuse reflectance of oceanic shallow waters: Influence of water depth and bottom albedo, *Limnol. Oceanogr.*, 39, 1689–1703, <https://doi.org/10.4319/lo.1994.39.7.1689>, 1994.
- Mobley, C. D.: *Light and water: Radiative transfer in natural waters*, Academic Press, San Diego, 1994.
- Pope, A., Scambos, T. A., Moussavi, M., Tedesco, M., Willis, M., Shean, D., and Grigsby, S.: Estimating supraglacial lake depth in West Greenland using Landsat 8 and comparison with other multispectral sensors, *The Cryosphere*, 10, 15–27, <https://doi.org/10.5194/tc-10-15-2016>, 2016.
- Pope, R. M. and Fry, E. S.: Absorption spectrum (380–700 nm) of pure water. II. Integrating cavity measurements, *Appl. Opt.*, 36, 8710–8723, <https://doi.org/10.1364/AO.36.008710>, 1997.
- Smith, R. C. and Baker, K. S.: Optical properties of the clearest natural waters (200–800 nm), *Appl. Opt.*, 20, 177–184, <https://doi.org/10.1364/AO.20.000177>, 1981.
- Sneed, W. A. and Hamilton, G. S.: Evolution of melt pond volume on the surface of the Greenland Ice Sheet, *Geophys. Res. Lett.*, 34, L03501, <https://doi.org/10.1029/2006GL028697>, 2007.